



# Terahertz Wave Absorption Property of all Mixed Organic–Inorganic Hybrid Perovskite Thin Film MA(Sn, Pb)(Br, I)<sub>3</sub> Fabricated by Sequential Vacuum Evaporation Method

Inhee Maeng<sup>1</sup>, Hiroshi Tanaka<sup>2</sup>, Valynn Katrine Mag-usara<sup>3</sup>, Makoto Nakajima<sup>3</sup>, Masakazu Nakamura<sup>2</sup> and Min-Cherl Jung<sup>4\*</sup>

<sup>1</sup>YUHS-KRIBB, Medical Convergence Research Institute, College of Medicine, Yonsei University, Seoul, South Korea, <sup>2</sup>Division of Materials Science, Nara Institute of Science and Technology, Ikoma, Japan, <sup>3</sup>Institute of Laser Engineering, Osaka University, Suita, Japan, <sup>4</sup>Division of Materials Science, Faculty of Pure and Applied Sciences, University of Tsukuba, Ibaraki, Japan

## OPEN ACCESS

### Edited by:

Rene A Nome,  
State University of Campinas, Brazil

### Reviewed by:

Jun Yin,  
King Abdullah University of Science  
and Technology, Saudi Arabia  
Sudhanshu Shukla,  
University of Luxembourg,  
Luxembourg

### \*Correspondence:

Min-Cherl Jung  
jung.mincherl.fp@u.tsukuba.ac.jp

### Specialty section:

This article was submitted to  
Physical Chemistry and Chemical  
Physics,  
a section of the journal  
Frontiers in Chemistry

Received: 04 August 2021

Accepted: 02 September 2021

Published: 16 September 2021

### Citation:

Maeng I, Tanaka H, Mag-usara VK,  
Nakajima M, Nakamura M and  
Jung M-C (2021) Terahertz Wave  
Absorption Property of all Mixed  
Organic–Inorganic Hybrid Perovskite  
Thin Film MA(Sn, Pb)(Br, I)<sub>3</sub> Fabricated  
by Sequential Vacuum  
Evaporation Method.  
Front. Chem. 9:753141.  
doi: 10.3389/fchem.2021.753141

All mixed hybrid perovskite (MA(Sn, Pb)(Br, I)<sub>3</sub>) thin film was fabricated by sequential vacuum evaporation method. To optimize the first layer with PbBr<sub>2</sub> and SnI<sub>2</sub>, we performed different annealing treatments. Further, MA(Sn, Pb)(Br, I)<sub>3</sub> thin film was synthesized on the optimized first layer by evaporating MAI and post-annealing. The formed hybrid perovskite thin film exhibited absorptions at 1.0 and 1.7 THz with small absorbance (<10%). Moreover, no chemical and structural defect-incorporated absorption was found. In this study, the possibility of changing terahertz absorption frequency through the mixture of metal cations (Sn<sup>+</sup> and Pb<sup>+</sup>) and halogen anions (Br<sup>-</sup> and I<sup>-</sup>) was verified.

**Keywords:** sequential vacuum evaporation, atomic structure, chemical state, THz-wave absorption, MA(Sn, Pb)(Br I)<sub>3</sub>

## INTRODUCTION

Recently, organic–inorganic hybrid perovskite (OHP) materials, because of their universal properties such as controllable bandgap, weak exciton binding energy, and high-carrier mobility, are attracting great attention for solar-cell and light-emitting diode applications (D’Innocenzo et al., 2014; Frost et al., 2014; Frost and Walsh, 2016; Pedesseau, 2016; NR Venkatesan, 2018; Yi et al., 2019). Many researchers are focusing on their fundamental properties to explore possibilities of new applications such as laser, memory device, and terahertz (THz) detector (ER Dohner, 2014; Kepenekian et al., 2015; Saba et al., 2016; Srimath Kandada and Petrozza, 2016; Lee et al., 2018; Sarritzu et al., 2018; Straus and Kagan, 2018; Grancini and Nazeeruddin, 2019; Obraztsov et al., 2021). In fact, the versatility of OHP contains very high possibility in novel device applications. One of new possibilities using OHP is THz-based application because OHP is composed of perovskite structure between organic and inorganic portions. In principle, the OHP structure is supposed to possess both molecular vibrations from the organic portion and lattice vibrations from the inorganic portion (Park et al., 2016).

To realize a THz-based application using OHP materials, two phonon modes such as molecule cation and metal cation–halogen anion vibrations in the THz range from 0.5 to 3 THz are primarily investigated (La-O-Vorakiat et al., 2016; Zhao et al., 2017; Cinquanta et al., 2019; Lee et al., 2019; Maeng et al., 2020b, 2020a). Further, the molecular motions (rotation and translation) of the CH<sub>3</sub>NH<sub>3</sub><sup>+</sup> (MA<sup>+</sup>) ion, which were confirmed by powder neutron diffraction, were found to be ordered, whereas the 2D and 3D disorder was dependent on each structure being controlled by temperature (Weller et al., 2015). However, there is no report on the

experimental observation of the molecular vibration and rotation in  $\text{CH}_3\text{NH}_3\text{PbI}_3$  (MAPbI<sub>3</sub>) and  $\alpha\text{-HC(NH}_2)_2\text{PbI}_3$  ( $\alpha\text{-FAPbI}_3$ ) thin films (Lee et al., 2019; Maeng et al., 2019). Possibly, the contribution of molecular motions is considerably weak in the THz energy range from 0.5 to 3 THz. In MAPbI<sub>3</sub> thin films fabricated by a conventional solution-based method, two vibrational modes at 1 and 2 THz, originated from the buckling of the Pb–I–Pb angles and the Pb–I bond vibration, respectively, were observed (La-O-Vorakiat et al., 2016). Additionally, a high THz-wave absorption at 1.58 THz was observed in MAPbI<sub>3</sub> thin film fabricated by sequential vacuum evaporation (SVE) method, which incorporated  $\text{CH}_3\text{NH}_2$  molecular defects in the synthesized thin film (Maeng et al., 2019; 2020b). Our recent reports indicate that a vacuum-processed method such as SVE creates a greater number of variable atomic and chemical states than a solution-processed method because vacuum-processed methods produce smaller grains, a higher density of grain boundaries and defects (Jung et al., 2018; Lee et al., 2019; Maeng et al., 2020a, 2020b). Generally, the thin films formed by solution-processed methods such as 2-step and antisolvent methods are shown with two significant features such as large grain size (>500 nm) and low density of grain boundary that are induced with high carrier mobility in a solar-cell application (Ono and Qi, 2016, 2018). In the case of the vacuum-processed methods such as co-evaporation and SVE, it shows a relatively small grain size (<200~300 nm) and a high density of grain boundary. The annealing process is very important to improve the quality of thin films fabricated by vacuum-processed methods. However, it causes to deplete elements on the surface and makes an unstable stoichiometry. (Ono and Qi, 2016). Also, the grain size does not improve significantly (Lee et al., 2019; Maeng et al., 2020a, 2020b).

To confirm the origins of various THz absorptions in OHP thin film, different composition elements for metal cation and halogen anion such as Sn and Br need to be investigated. In addition, a study on OHP thin films with mixtures of metal cations as well as

halogen anions will be significantly interesting because of a modulation possibility of absorption frequency which can be an essential function for THz-detector or -modulator.

In this study, we fabricated and characterized an all mixed hybrid perovskite,  $\text{MA}(\text{Sn, Pb})(\text{Br, I})_3$ . First, we optimized the first layer with lead (II) bromide ( $\text{PbBr}_2$ ) and tin (II) iodide ( $\text{SnI}_2$ ) using SVE method. Next,  $\text{MA}(\text{Sn, Pb})(\text{Br, I})_3$  thin film was formed by evaporating MAI in the same method. In the THz time domain spectroscopy (THz-TDS), the formed hybrid perovskite thin film exhibited 1.0 and 1.7 THz absorptions, and there was no chemical and structural defect-incorporated absorption.

## MATERIAL AND METHODS

OHP thin films were fabricated by SVE in a customized vacuum chamber. A polyethylene terephthalate (PET) flexible substrate (AHCF-100, thickness = 225  $\mu\text{m}$ , AIDEN) was cleaned by sonication in acetone for 10 min, rinsed in heated acetone for 1 min, and then treated in a UV-ozone chamber for 30 min before finally loading it into a vacuum chamber. To fabricate all mixed organic–inorganic hybrid perovskite thin film using SVE, first, we optimized the first mixed layers with  $\text{SnI}_2$  and  $\text{PbBr}_2$ . The SVE chamber had two heaters for separate evaporations of  $\text{SnI}_2$  and  $\text{PbBr}_2$ . The base pressure was  $8.0 \times 10^{-3}$  Pa. First,  $\text{SnI}_2$  (Sigma-Aldrich, 99.99% purity) was evaporated onto the substrates at room temperature with a fixed deposition rate and thickness of 10  $\text{\AA}/\text{s}$  and 50 nm, respectively, (Jung et al., 2018). Next, we evaporated  $\text{PbBr}_2$  (Sigma-Aldrich, > 99.8% purity) onto the substrates with same deposition rate and thickness (Jung et al., 2018). Finally, we performed separate post-annealing at 110°C for 10, 20, and 45 min, respectively, of three fabricated films in an  $\text{N}_2$  glovebox to find an optimized mixed thin film (Figure 1).

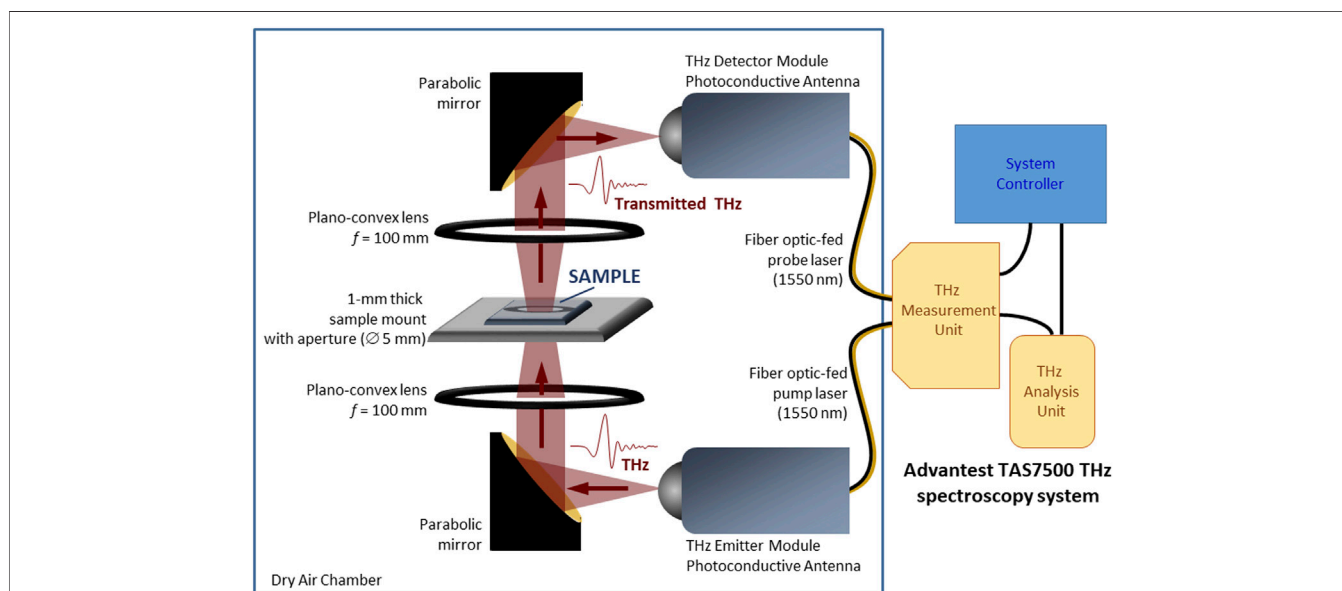


**FIGURE 1** | The transmission terahertz time-domain spectroscopy (THz-TDS) system used for investigating the transmittance of the hybrid perovskite samples (This schematic is not drawn to scale.)

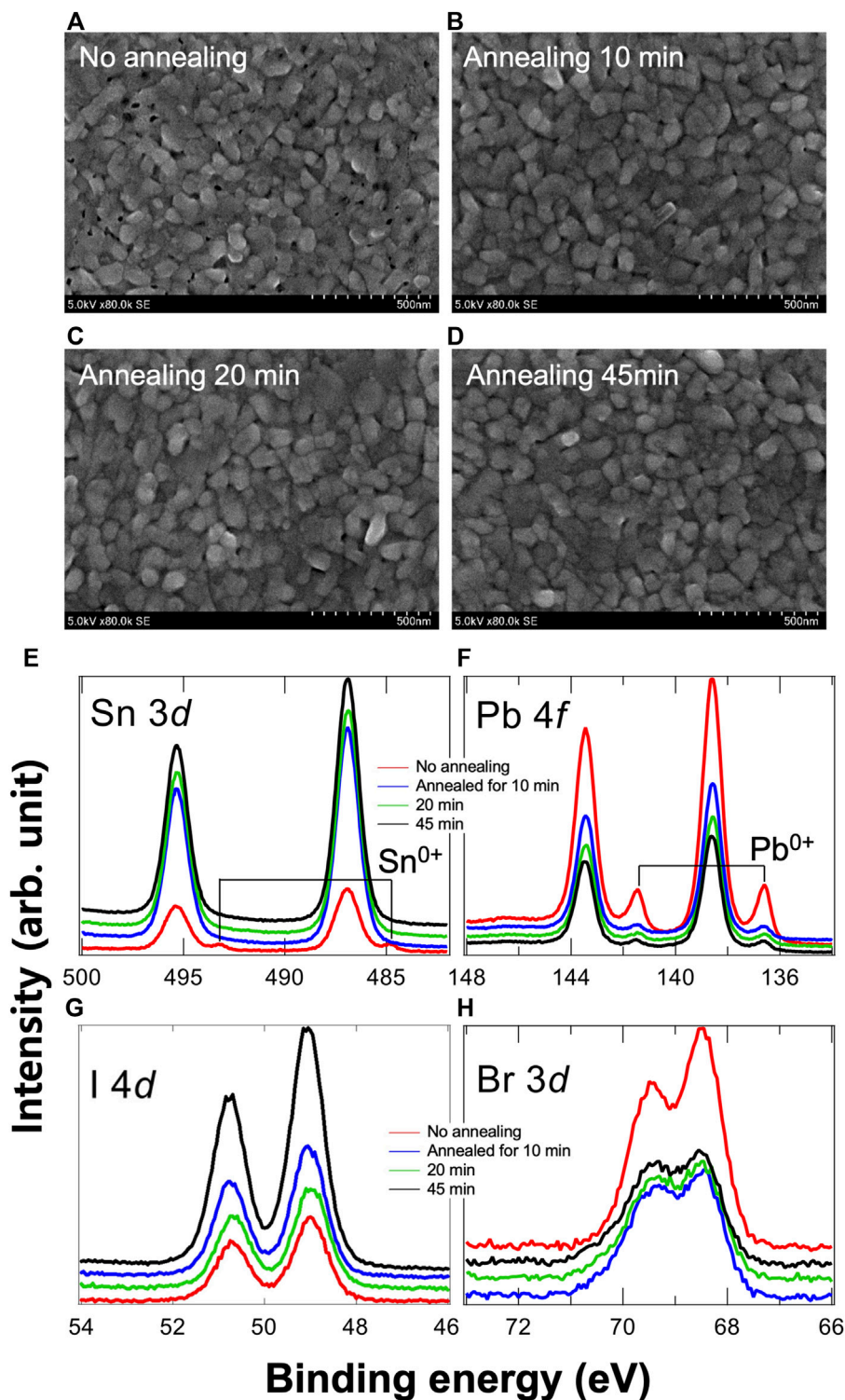


**FIGURE 2** | Surface morphologies of PbBr<sub>2</sub>/SnI<sub>2</sub> after (A) no-annealing, (B) 10-min annealing, (C) 20-min annealing, and (D) 45-min annealing treatments. The grain sizes do not show any significant change. Additionally, the vacant area disappears after annealing. Chemical states of (E) Sn 3d, (F) Pb 4f, (G) I 4d, and (H) Br 3d core-levels. Because of the annealing process, we confirm that a physical mixture of PbBr<sub>2</sub>/SnI<sub>2</sub> is formed because there is no new chemical state, and changes in the peak intensities only are observed.

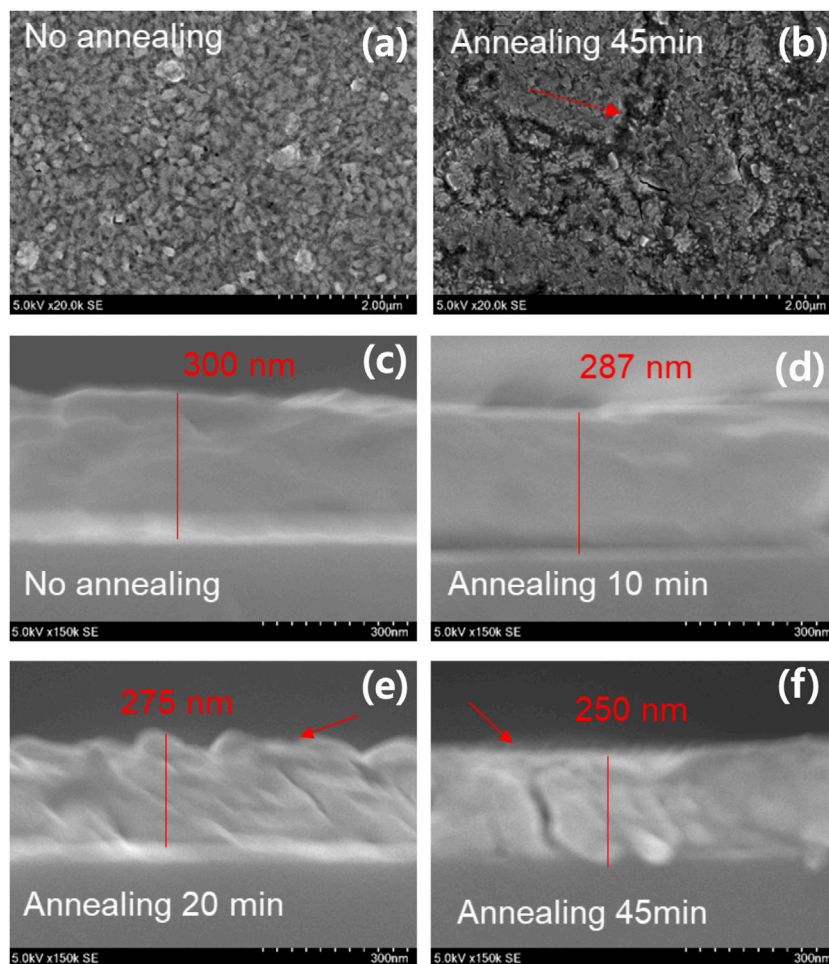


**FIGURE 3** | Surface morphologies after the deposition of MAI of **(A)** no-annealing and **(B)** 45-min annealing samples. The surface is dramatically changed with the appearance of a valley. **(C–F)** Additionally, the thickness decreases from 300 to 250 nm with increase in the annealed time. The deep void can be observed in both the 20- and 45-min annealing samples.

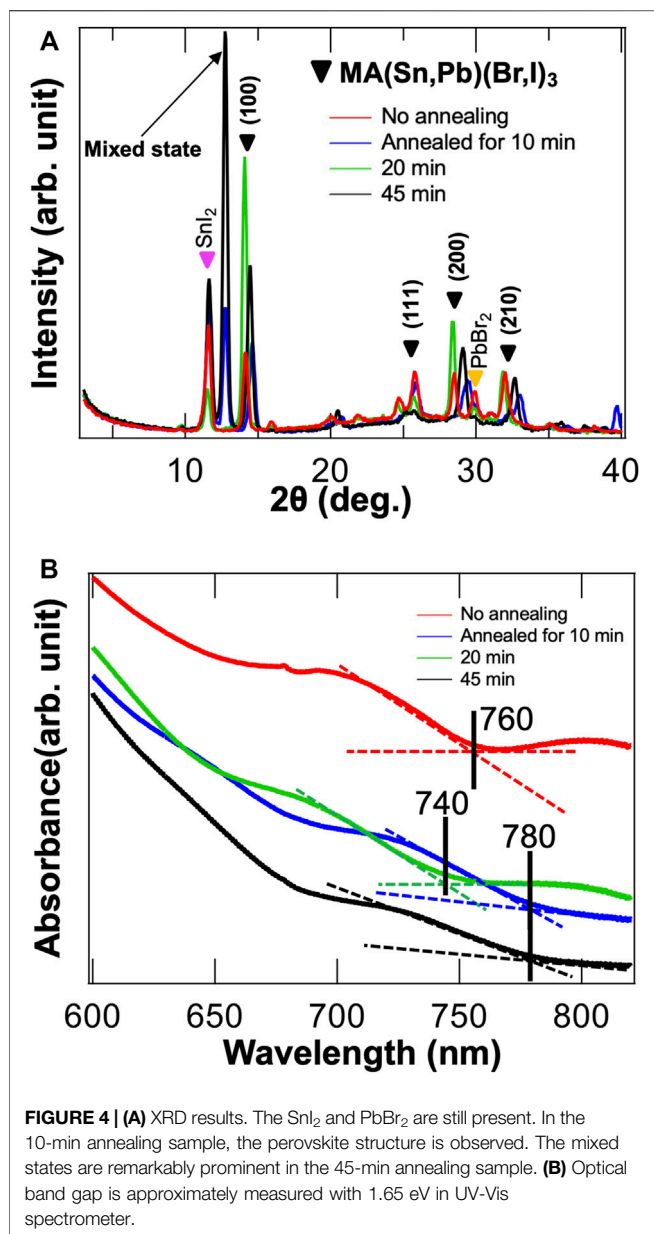
From this first optimization, we selected the sample post-annealed for 10 min. The mixed layer with  $\text{SnI}_2/\text{PbBr}_2$  was further deposited with  $\text{CH}_3\text{NH}_3\text{I}$  (Methylammonium iodide, MAI, Sigma-Aldrich, 98% purity) with a fixed deposition rate and thickness of  $2 \text{ \AA}/\text{s}$  and 300 nm, respectively, (Jung et al., 2018). Again, we performed separate post-annealing at  $110^\circ\text{C}$  for 10, 20, and 45 min, respectively, in an  $\text{N}_2$  glovebox to form final organic–inorganic hybrid perovskite structures.

To protect the formed thin films against air and water, finally, spin coating was applied at 4 krpm for 1 min to coat all thin films with a PTAA (Sigma-Aldrich) solution containing 5 mg PTAA and 4 ml chlorobenzene. The PTAA solution was sonicated for 1 h (Lee et al., 2019; Maeng et al., 2020a).

To characterize the formed thin films, we performed scanning electron microscopy (SEM), X-ray diffraction (XRD), and X-ray photoelectron spectroscopy (XPS). SEM characterization was conducted at an acceleration voltage of 5 keV and an emission current of  $10 \mu\text{A}$  using HITACHI SU9000. The XRD instrument was RINT-TTRIII/NM with a  $\text{Cu } K_\alpha$  source constructed by

Rigaku. All XPS measurements were performed using Versa ProbeII with a monochromated  $\text{AlK}_\alpha$  (ULVAC-PHI) to obtain  $\text{Pb } 4f$ ,  $\text{I } 4d$ ,  $\text{Sn } 3d$ ,  $\text{Br } 3d$  core-levels, and valence spectra. Binding energies were calibrated with respect to the  $\text{Au } 4f_{7/2}$  core-level (84.0 eV) (Wagner et al., 1995).

Transmission type THz-TDS was utilized to characterize the samples and elucidate their THz-wave absorption properties. (Nakajima et al., 2008; Nakajima et al., 2009; Nakajima et al., 2016; Jung et al., 2018; Ohkoshi et al., 2020; Agulto et al., 2021; Fitzky et al., 2021). Transmittances of the samples were obtained by non-destructive testing and analysis using an Advantest TAS7500 THz spectroscopy system, which allowed the direct measurement of time-domain THz waveforms and the corresponding power spectra at room temperature ( $22 \pm 1^\circ\text{C}$ ) and dry air (relative humidity  $<1.5\%$ ) conditions. The system, which had a spectral resolution of 7.6 GHz, was equipped with a photoconductive antenna (PCA) for THz emission, a sample holder, and another PCA for the detection of transmitted THz radiation through the sample. For all THz transmission



measurements, each sample was mounted on a sample holder with 5-mm-diameter aperture at a fixed optimum distance between the two PCAs, and measurements with only the substrate as well as without any sample on the sample holder were also performed for reference. The transmittance was subsequently acquired by comparing the transmission spectra of each sample with the corresponding reference spectra. The schematic of the THz-TDS system is shown in **Figure 1**.

## RESULTS AND DISCUSSION

To find an optimized mixed thin film with  $\text{PbBr}_2/\text{SnI}_2$ , we performed the post-annealing with different annealing times. Drastic changes in the surface morphologies and chemical

states after the annealing treatments are shown. (**Figure 2**). From the SEM results, it can be observed that the grain sizes, which are in the range of 80–120 nm, do not change significantly for different post-annealing times. However, the vacant areas disappeared with increased post-annealing time. (**Figures 2A–D**). Interestingly, all XPS intensities change dramatically for the samples annealed for 10 min and more. The intensities corresponding to Sn 3s and I 4d core-levels increase, (**Figures 2E,G**), whereas the intensities corresponding to Pb 4f and Br 4d core-levels decrease, (**Figures 2F,H**), indicating that the bottom  $\text{SnI}_2$  and upper  $\text{PbBr}_2$  are out- and in-diffused to the surface and bulk, respectively. As the annealing time increases, this trend becomes more prominent. Notably, no new chemical state is observed during annealing. Based on these observations, we confirmed the following:

- 1) Initially formed thin film structure had physical separation between  $\text{SnI}_2$  and  $\text{PbBr}_2$ .

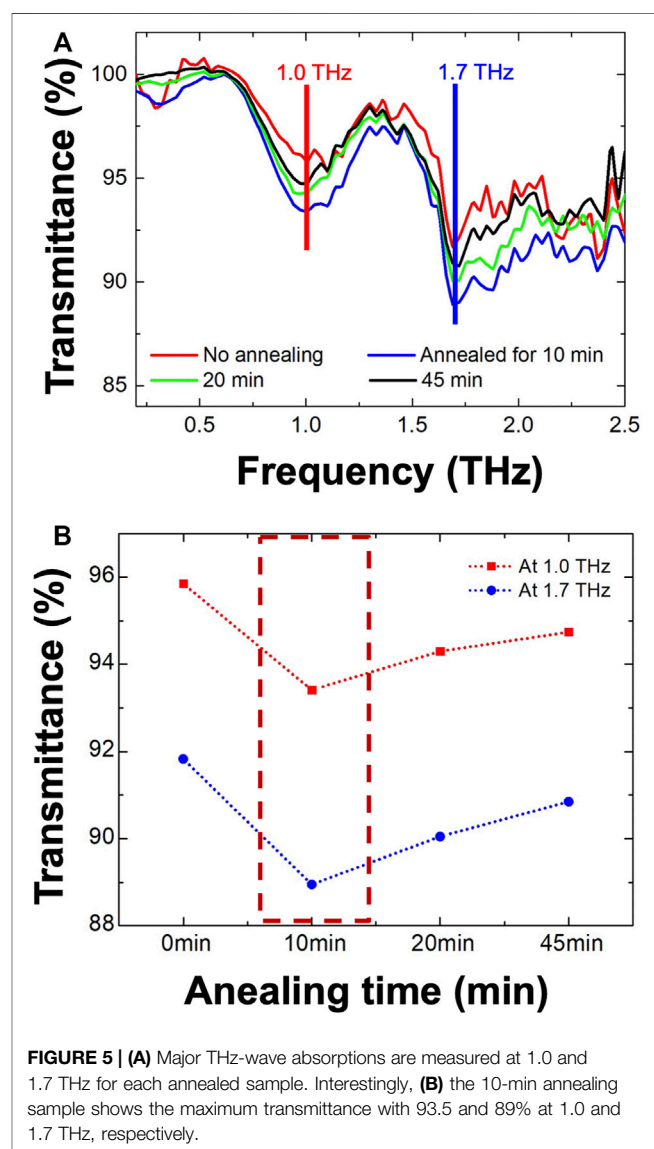


**TABLE 1** | Comparison of THz-wave absorption properties of each perovskite thin film.

Sample	Peak 1 (buckling vibration)	Peak 2 (translation vibration)	Peak 3	Lattice constant (Å)	Crystal structure (RT)
MA(Sn,Pb)(Br,I) <sub>3</sub>	1.0 THz	1.7 THz	No peak	6.20	Cubic
MAPbI <sub>3</sub> Maeng et al. (2019)	0.95 THz	1.87 THz	1.58 THz (Defect-incorporated)	6.27	Tetra
MAPbBr <sub>3</sub> Maeng et al. (2020a)	0.85 THz	1.38 THz	2.00 THz (Br self-vibration)	5.95	Cubic
MASnI <sub>3</sub> Li and Rinke. (2016)		There is no significant THz-wave absorption		6.23	Cubic

2) The post-annealing process induced a physically mixed layer of SnI<sub>2</sub> and PbBr<sub>2</sub>.

Additionally, the chemical states of Sn<sup>0+</sup> and Pb<sup>0+</sup> were observed for the no-annealing sample. However, they soon disappeared as the post-annealing process was initiated. Although there was still a small trace of Pb<sup>0+</sup> after annealing, the annealing process almost induced a depletion of non-stoichiometry elements in the thin film. For the next deposition step, the optimized thin film is required with a rough stacking structure (Jung et al., 2018). We selected the 10-min annealing sample because if the thin film was dense, the second element, MAI, would not be able to penetrate the bulk (Jung et al., 2018).

To obtain all mixed OHP thin film, we performed the post-annealing with different annealing times such as 10, 20, and 45 min after evaporating MAI. We observe different surface morphologies for the no- and 45-min annealing samples. (Figures 3A,B). For the 45-min annealing sample, we notice a profound crack on the surface (indicated by the red arrow). (Figure 3B). Interestingly, the film thickness, along the cross-sectional view of the thin film, decreases from 300 to 250 nm as the annealing time increases. (Figures 3C–F). Moreover, we confirm that the observed crack in the 45-min annealing sample reaches from surface to bulk (red arrow). This crack started to appear in the 20-min annealing sample. Interestingly, we did not find any cracked structure in the 10-min annealing sample.

To confirm the atomic structure, we performed XRD and UV-Vis measurements. (Figure 4). Interestingly, SnI<sub>2</sub> and PbBr<sub>2</sub> components are still observed in the XRD results. The mixed state, which was incorporated with the CH<sub>3</sub>NH<sub>2</sub> molecular defect, increases dramatically for an annealing period of 20 min and more (Jung et al., 2018; Maeng et al., 2020b, 2020b). From these results, we can confirm that owing to the presence of cracks and remaining constituent elements, the formation of all mixed perovskite structure in a thin film is difficult using SVE. However, the 10 and 20-min annealing samples exhibited relatively small intensities for SnI<sub>2</sub>, PbBr<sub>2</sub>, and mixed state. Unfortunately, it is very difficult to determine an exact stoichiometry of our formed hybrid perovskite thin film from XRD results. In the UV-Vis measurements, the optical absorptions of the no-annealing, 10-min, 20-min, and 45-min annealing samples are 760, 740, 780, and 780 nm, respectively,

(Figure 4B). We did not observe any change in the optical absorption after the 20-min annealing treatment.

To explore the THz-wave absorption property, we performed THz-TDS experiment. Although the absorbance does not appear to be strong, we observe two prominent absorptions at 1.0 and 1.7 THz for all samples. (Figure 5A). After annealing for 10 min, the absorption property improves slightly. (Figure 4B). However, the transmittance increases as the annealing time is increased further. (Figure 5B). Consistently with the XRD results, it shows a degradation of perovskite structure after the 10-min annealing process. According to our previous studies, the 1.0 and 1.7 THz absorptions are assumed to originate from buckling and translation vibrations, respectively, (Maeng et al., 2019; 2020a). However, we did not observe any additional absorption such as defect-incorporated structure or Br self-vibration. (Maeng et al., 2019; 2020a). To compare with MAPbI<sub>3</sub> and MAPbBr<sub>3</sub>, we have summarized various parameters related to THz-wave absorption in Table 1.

Interestingly, the lattice constant of the formed MA(Sn, Pb)(Br,I)<sub>3</sub> is 6.20 Å, which is an intermediate value between the lattice constant values of MAPbI<sub>3</sub> (6.27 Å) and MAPbBr<sub>3</sub> (5.95 Å). Furthermore, we have confirmed that the THz-wave absorptions of MA(Sn, Pb)(Br,I)<sub>3</sub> are different in comparison with those of MAPbI<sub>3</sub> and MAPbBr<sub>3</sub>. (Table 1). Unfortunately, we did not observe any significant THz-wave absorption in MASnI<sub>3</sub>, indicating a lack of clarity regarding the effect of Sn. In short, the origin of this increased absorption frequency is not easy to understand. However, we demonstrated that the fabricated mixed hybrid perovskite changes the frequencies of THz-wave absorptions.

## CONCLUSION

We fabricated MA(Sn, Pb)(Br, I)<sub>3</sub> by SVE in this study. Although the formed thin films were subjected to different annealing treatments, further optimizations are required in the thin film fabrication process. However, we verified the possibility of THz-wave absorption changes due to the mixture of metal cations (Sn<sup>+</sup> and Pb<sup>+</sup>) and halogen anions (Br<sup>-</sup> and I<sup>-</sup>). To be a candidate material for THz-based application such as sensing and modulating devices, we believe this confirmation is a first step for the frequency modulating by the element mixtures.

## DATA AVAILABILITY STATEMENT

The raw data supporting the conclusions of this article will be made available by the authors, without undue reservation.

## AUTHOR CONTRIBUTIONS

M-CJ conceived the idea, designed the experiments, and supervised the project. IM and HT performed a major portion of the sample preparation and characterization. VKM and MN performed the

THz-TDS experiment. All authors discussed the results, performed data analysis and explanation, wrote the article, and revised it.

## FUNDING

This work was supported by funding from the program of research grant 2020 of Izumi Zaidan (Japan). This work was also supported by the Basic Science Research Program (NRF-2020R1C1C1013646) through the NRF funded by the Korean Ministry of Education.

## REFERENCE

- Agulto, V. C., Toya, K., Phan, T. N. K., Mag-usara, V. K., Li, J., Empizo, M. J. F., et al. (2021). Anisotropic Complex Refractive Index of  $\beta$ -Ga<sub>2</sub>O<sub>3</sub> Bulk And Epilayer Evaluated By Terahertz Time-Domain Spectroscopy. *Appl. Phys. Lett.* 118, 042101. doi:10.1063/5.0031531
- Cinquanta, E., Meggiolaro, D., Motti, S. G., Gandini, M., Alcocer, M. J. P., Akkerman, Q. A., et al. (2019). Ultrafast THz Probe of Photoinduced Polarons in Lead-Halide Perovskites. *Phys. Rev. Lett.* 122, 166601. doi:10.1103/PhysRevLett.122.166601
- D'Innocenzo, V., Srimath Kandada, A. R., de Bastiani, M., Gandini, M., and Petrozza, A. (2014). Tuning the Light Emission Properties by Band gap Engineering in Hybrid lead Halide Perovskite. *J. Am. Chem. Soc.* 136, 17730–17733. doi:10.1021/ja511198f
- Dohner, E. R., Jaffe, A., Bradshaw, L. R., and Karunadasa, H. I. (2014). Intrinsic white-light Emission from Layered Hybrid Perovskites. *J. Am. Chem. Soc.* 136, 13154–13157. doi:10.1021/ja507086b
- Fitzky, G., Nakajima, M., Koike, Y., Leitenstorfer, A., and Kurihara, T. (2021). Ultrafast Control of Magnetic Anisotropy by Resonant Excitation of 4f Electrons and Phonons in Sm<sub>0.7</sub>Er<sub>0.3</sub>FeO<sub>3</sub>. *Phys. Rev. Lett.* 127, 107401. doi:10.1103/PhysRevLett.127.107401
- Frost, J. M., Butler, K. T., Brivio, F., Hendon, C. H., van Schilfgaarde, M., and Walsh, A. (2014). Atomistic Origins of High-Performance in Hybrid Halide Perovskite Solar Cells. *Nano Lett.* 14, 2584–2590. doi:10.1021/nl500390f
- Frost, J. M., and Walsh, A. (2016). What Is Moving in Hybrid Halide Perovskite Solar Cells? *Acc. Chem. Res.* 49, 528–535. doi:10.1021/acs.accounts.5b00431
- Grancini, G., and Nazeeruddin, M. K. (2019). Dimensional Tailoring of Hybrid Perovskites for Photovoltaics. *Nat. Rev. Mater.* 4, 4–22. doi:10.1038/s41578-018-0065-0
- Jung, M.-C., Kobori, S., Matsuyama, A., Maeng, I., Lee, Y. M., Kojima, H., et al. (2018). Formation of CH<sub>3</sub>NH<sub>2</sub>-incorporated Intermediate State in CH<sub>3</sub>NH<sub>3</sub>PbI<sub>3</sub> Hybrid Perovskite Thin Film Formed by Sequential Vacuum Evaporation. *Appl. Phys. Express* 12, 015501. doi:10.7567/1882-0786/aaf0ac
- Kepenekian, M., Robles, R., Katan, C., Saporì, D., Pedesseau, L., and Even, J. (2015). Rashba and Dresselhaus Effects in Hybrid Organic-Inorganic Perovskites: From Basics to Devices. *ACS Nano* 9, 11557–11567. doi:10.1021/acsnano.5b04409
- La-O-Vorakiat, C., Xia, H., Kadro, J., Salim, T., Zhao, D., Ahmed, T., et al. (2016). Phonon Mode Transformation across the Orthorhombic-Tetragonal Phase Transition in a Lead Iodide Perovskite CH<sub>3</sub>NH<sub>3</sub>PbI<sub>3</sub>: A Terahertz Time-Domain Spectroscopy Approach. *J. Phys. Chem. Lett.* 7, 1–6. doi:10.1021/acs.jpcclett.5b02223
- Lee, Y. M., Maeng, I., Park, J., Song, M., Yun, J.-H., Jung, M.-C., et al. (2018). Comprehensive Understanding and Controlling the Defect Structures: An Effective Approach for Organic-Inorganic Hybrid Perovskite-Based Solar-Cell Application. *Front. Energ. Res.* 6. doi:10.3389/fenrg.2018.00128
- Lee, Y. M., Yun, J.-H., Matsuyama, A., Kobori, S., Maeng, I., Lyu, M., et al. (2019). Significant THz-Wave Absorption Property in Mixed  $\delta$ - and  $\alpha$ -FAPbI<sub>3</sub> Hybrid Perovskite Flexible Thin Film Formed by Sequential Vacuum Evaporation. *Appl. Phys. Express* 12, 051003. doi:10.7567/1882-0786/ab0eec
- Li, J., and Rinke, P. (2016). Atomic Structure of Metal-Halide Perovskites from First Principles: The Chicken-And-Egg Paradox of the Organic-Inorganic Interaction. *Phys. Rev. B* 94, 045201. doi:10.1103/PhysRevB.94.045201
- Maeng, I., Lee, S., Tanaka, H., Yun, J.-H., Wang, S., Nakamura, M., et al. (2020a). Unique Phonon Modes of a CH<sub>3</sub>NH<sub>3</sub>PbBr<sub>3</sub> Hybrid Perovskite Film without the Influence of Defect Structures: an Attempt toward a Novel THz-Based Application. *NPG Asia Mater.* 12, 1–7. doi:10.1038/s41427-020-0235-6
- Maeng, I., Lee, Y. M., Park, J., Raga, S. R., Kang, C., Kee, C.-S., et al. (2019). Significant THz Absorption in CH<sub>3</sub>NH<sub>2</sub> Molecular Defect-Incorporated Organic-Inorganic Hybrid Perovskite Thin Film. *Sci. Rep.* 9, 5811. doi:10.1038/s41598-019-42359-8
- Maeng, I., Matsuyama, A., Yun, J.-H., Wang, S., Kang, C., Kee, C.-S., et al. (2020b). Strong Linear Correlation between CH<sub>3</sub>NH<sub>2</sub> Molecular Defect and THz-Wave Absorption in CH<sub>3</sub>NH<sub>3</sub>PbI<sub>3</sub> Hybrid Perovskite Thin Film. *Nanomaterials* 10, 721. doi:10.3390/nano10040721
- Nakajima, M., Takubo, N., Hiroi, Z., Ueda, Y., and Suemoto, T. (2008). Photoinduced Metallic State In VO<sub>2</sub> Proved By The Terahertz Pump-Probe Spectroscopy. *Appl. Phys. Lett.* 92, 011907. doi:10.1063/1.2830664
- Nakajima, M., Takubo, N., Hiroi, Z., Ueda, Y., and Suemoto, T. (2009). Study of Photo-Induced Phenomena in VO<sub>2</sub> by Terahertz Pump-Probe Spectroscopy. *J. Lumin.* 129, 1802. doi:10.1016/j.jlumin.2009.04.091
- Nakajima, M., Kurihara, T., Tadokoro, Y., Kang, B., Takano, K., and Yamaguchi, K. (2016). Application of Terahertz Field Enhancement Effect in Metal Microstructures. *J. Infra. Millim. Tera. Waves* 37, 1199. doi:10.1007/s10762-016-0323-4
- Obraztsov, P. A., Bulgakova, V. v., Chizhov, P. A., Ushakov, A. A., Gets, D. S., Makarov, S. v., et al. (2021). Hybrid Perovskite Terahertz Photoconductive Antenna. *Nanomaterials* 11, 313–411. doi:10.3390/nano11020313
- Ohkoshi, S., Yoshikiyo, M., Imoto, K., Nakagawa, K., Namai, A., and Tokoro, H. (2020). Magnetic Pole Flip By Millimeter Wave. *Adv. Mater.* 32, 2004897. doi:10.1002/adma.202004897
- Ono, L. K., and Qi, Y. (2018). Research Progress on Organic-Inorganic Halide Perovskite Materials and Solar Cells. *J. Phys. D: Appl. Phys.* 51, 093001. doi:10.1088/1361-6463/aaa727
- Ono, L. K., and Qi, Y. (2016). Surface and Interface Aspects of Organometal Halide Perovskite Materials and Solar Cells. *J. Phys. Chem. Lett.* 7, 4764–4794. doi:10.1021/acs.jpcclett.6b01951
- Park, N. G., Grätzel, M., and Miyasaka, T. (2016). *Organic-inorganic Halide Perovskite Photovoltaics: From Fundamentals to Device Architectures*. Springer. doi:10.1007/978-3-319-35114-8
- Pedesseau, L., Saporì, D., Traore, B., Robles, R., Fang, H.-H., Loi, M. A., et al. (2016). Advances and Promises of Layered Halide Hybrid Perovskite Semiconductors. *ACS Nano* 10, 9776–9786. doi:10.1021/acsnano.6b05944
- Saba, M., Quochi, F., Mura, A., and Bongiovanni, G. (2016). Excited State Properties of Hybrid Perovskites. *Acc. Chem. Res.* 49, 166–173. doi:10.1021/acs.accounts.5b00445
- Sarritzu, V., Sestu, N., Marongiu, D., Chang, X., Wang, Q., Masi, S., et al. (2018). Direct or Indirect Bandgap in Hybrid Lead Halide Perovskites? *Adv. Opt. Mater.* 6, 1701254. doi:10.1002/adom.201701254
- Srimath Kandada, A. R., and Petrozza, A. (2016). Photophysics of Hybrid Lead Halide Perovskites: The Role of Microstructure. *Acc. Chem. Res.* 49, 536–544. doi:10.1021/acs.accounts.5b00464
- Straus, D. B., and Kagan, C. R. (2018). Electrons, Excitons, and Phonons in Two-Dimensional Hybrid Perovskites: Connecting Structural, Optical, and Electronic Properties. *J. Phys. Chem. Lett.* 9, 1434–1447. doi:10.1021/acs.jpcclett.8b00201
- Venkatesan, N. R., Labram, J. G., and Chabincyn, M. L. (2018). Charge-Carrier Dynamics and Crystalline Texture of Layered Ruddlesden-Popper Hybrid Lead Iodide Perovskite Thin Films. *ACS Energ. Lett.* 3, 380–386. doi:10.1021/acsenerylett.7b01245

- Wagner, C. D., Riggs, W. M., Davis, L. E., Moulder, J. F., and Muilenberg, G. E. (1995). Handbook of X-ray Photoelectron Spectroscopy: a Reference Book of Standard Spectra for Identification and Interpretation of XPS Data - Catalog - UW-Madison Libraries. Available at: <https://search.library.wisc.edu/catalog/999931119402121>.
- Weller, M. T., Weber, O. J., Henry, P. F., di Pumpo, A. M., and Hansen, T. C. (2015). Complete Structure and Cation Orientation in the Perovskite Photovoltaic Methylammonium lead Iodide between 100 and 352 K. *Chem. Commun.* 51, 4180–4183. doi:10.1039/c4cc09944c
- Yi, Z., Ladi, N. H., Shai, X., Li, H., Shen, Y., and Wang, M. (2019). Will Organic-Inorganic Hybrid Halide lead Perovskites Be Eliminated from Optoelectronic Applications? *Nanoscale Adv.* 1, 1276–1289. doi:10.1039/c8na00416a
- Zhao, D., Skelton, J. M., Hu, H., La-O-Vorakiat, C., Zhu, J.-X., Marcus, R. A., et al. (2017). Low-frequency Optical Phonon Modes and Carrier Mobility in the Halide Perovskite CH<sub>3</sub>NH<sub>3</sub>PbBr<sub>3</sub> Using Terahertz Time-Domain Spectroscopy. *Appl. Phys. Lett.* 111, 201903. doi:10.1063/1.4993524

**Conflict of Interest:** The authors declare that the research was conducted in the absence of any commercial or financial relationships that could be construed as a potential conflict of interest.

**Publisher's Note:** All claims expressed in this article are solely those of the authors and do not necessarily represent those of their affiliated organizations, or those of the publisher, the editors and the reviewers. Any product that may be evaluated in this article, or claim that may be made by its manufacturer, is not guaranteed or endorsed by the publisher.

Copyright © 2021 Maeng, Tanaka, Mag-usara, Nakajima, Nakamura and Jung. This is an open-access article distributed under the terms of the Creative Commons Attribution License (CC BY). The use, distribution or reproduction in other forums is permitted, provided the original author(s) and the copyright owner(s) are credited and that the original publication in this journal is cited, in accordance with accepted academic practice. No use, distribution or reproduction is permitted which does not comply with these terms.